Applications. Chromium compounds have found commercial use for the polymerization of ethylene and propylene.[79–81] In aqueous solutions, ethylene is polymerized upon addition of $ArCH_2CrL(H_2O)^{2+}$, presumably by a chain reaction of $ArCH_2^{\bullet}$, formed by homolysis.[82] Other organochromium(III) compounds are also active catalysts for alkene polymerization, usually in organic solvents like CH_2Cl_2 and THF. This includes $[Cp^*Cr(THF)_3CH_3](BPh_4)$ and $[Cp^*Cr(CH_2SiMe_3)_2]$.[83]

Under certain circumstances, organochromium(III) compounds react with aldehydes, as in eq 13. This occurs for $RCrCl_2(THF)_3$, as shown.[84] Ketones are unreactive. The complexes $R_2CrCl(THF)_3$ also react, but $(H_2O)_5CrR^{2+}$ is unreactive.[85] The R groups used include CH_3, n-C_3H_7, n-C_4H_9, sec-C_4H_9, n-C_8H_{17}, and $PhCH_2$. Extensive tests were run for both heptanal and benzaldehyde.

$$RCrCl_2(THF)_3 + R'CHO \xrightarrow{H_2O} RR'CHOH + HOCrCl_2(THF)_3 \quad (13)$$

Another application for organochromium(III) complexes is found in their use for selective coupling of free radicals. Once some CrR^{2+} is formed, as in Scheme I, the radical may instead react with CrR^{2+}:

$$R^{\bullet} + CrR^{2+} \rightarrow \{CrR_2^{2+}\}\ (?) \rightarrow Cr^{2+} + R_2 \quad (14)$$

Reactant ratios must be chosen carefully, and conditions can even be arranged first to make CrR^{2+} and then, with a different alkyl halide, RR′. There is no evidence for the dialkylchromium(IV) intermediate pictured in eq 14. This reaction might also be viewed as an S_H2 displacement, although its mechanism has not been studied.

Concluding Remarks. The family of $(H_2O)_5CrR^{2+}$ complexes has provided remarkably fertile ground for mechanistic study. Many reactions display a range of reactivity. As shown, the CrR^{2+} bond dissociates both heterolytically and homolytically, and the balance between them can be controlled. That is, for a given R, homolysis can be promoted by addition of a scavenger and retarded by added Cr^{2+}. Similarly, increasing steric bulk on the α-carbon greatly increases the rate of homolysis but accelerates heterolysis only marginally. Because the proton and the solvent are kinetically inefficient electrophiles, the complexes survive in aqueous media. More reactive electrophiles, such as mercuric salts or halogens, react very rapidly.

These complexes, or closely related ones, have recently been shown to have promise in organic reactions.[86] They can initiate olefin polymerization and can add nucleophilically to aldehydes.

I am grateful for the collaborations of many co-workers, cited in the footnotes. This research was supported by the Chemical Sciences Division, Office of Basic Energy Sciences, U.S. Department of Energy, under Contract W-7405-Eng-82.

(78) Sauer, A.; Cohen, H.; Meyerstein, D. *Inorg. Chem.* **1988**, *27*, 4578.
(79) Clark, A. *Catal. Rev.* **1969**, *3*, 145.
(80) Karol, F. *J. Catal. Rev. Sci. Eng.* **1984**, *26*, 557.
(81) Sinn, H.; Kaminsky, W. *Adv. Organomet. Chem.* **1980**, *18*, 99.
(82) Shi, S. Unpublished observations.
(83) Thomas, B. J.; Theopold, K. H. *J. Am. Chem. Soc.* **1988**, *110*, 5902.
(84) Kauffmann, T.; Hamsen, A.; Beirich, C. *Angew. Chem., Int. Ed. Engl.* **1982**, *21*, 144.
(85) Kauffmann, T.; Abeln, R.; Wingbermühle, D. *Angew. Chem., Int. Ed. Engl.* **1984**, *23*, 729.
(86) Muzart, J. *Chem. Rev.* **1992**, *92*, 113.

The Transient Grating: A Holographic Window to Dynamic Processes

JOHN T. FOURKAS† and M. D. FAYER*

Department of Chemistry, Stanford University, Stanford, California 94305

Received October 2, 1991

Introduction

As laser technology progresses, nonlinear optical (NLO) techniques[1] are becoming increasingly important tools in chemistry. Most NLO techniques involve several laser beams and a distinct signal beam; however, the single defining characteristic of a NLO experiment is that the intensity of the observed signal is proportional to the nth power of the laser intensity, where $n > 1$. Examples of NLO techniques that have been used in chemistry include the photon echo,[2] second-harominc generation,[3] and hole burning.[4,5] In this Account we discuss what has become perhaps the most widely used NLO technique in chemistry, the transient grating (TG).[6,7] TG experiments have been performed in all

John Fourkas was born in Alameda, CA. He obtained a B.S. (1986) and an M.S. (1986) in chemistry from the California Institute of Technology and a Ph.D. (1992) in chemistry from Stanford University. He is presently a postdoctoral researcher at the University of Texas at Austin.

Michael Fayer was born in Los Angeles, Ca. He obtained a B.S. (1969) and a Ph.D. (1974) from the University of California, Berkeley. He joined the faculty at Stanford University in 1974 and has been a full professor there since 1984. His research interests include intermolecular interactions and dynamics in condensed-matter systems, investigated with ultrafast nonlinear optical methods, conventional spectroscopy, and theoretical methods.

†Present address: Department of Chemistry and Biochemistry, University of Texas at Austin, Austin, TX 78712.

(1) Levenson, M. D.; Kano, S. S. *Introduction to Nonlinear Laser Spectroscopy*; Academic Press: Boston, 1988; pp 299.
(2) Walsh, C. A.; Berg, M.; Narasimhan, L. R.; Fayer, M. D. *Acc. Chem. Res.* **1987**, *20*, 120.
(3) Richmond, G. L.; Robinson, J. M.; Shannon, V. L. *Prog. Surf. Sci.* **1988**, *28*, 1.
(4) *Persistent Spectral Holeburning: Science and Applications*; Moerner, W. E., Ed.; Springer: New York, 1988.
(5) Berg, M.; Walsh, C. A.; Narasimhan, L. R.; Littau, K. A.; Fayer, M. D. *J. Chem. Phys.* **1988**, *88*, 1564.
(6) Eichler, H. J.; Günter, P.; Pohl, D. W. *Laser-Induced Dynamic Gratings*; Springer-Verlag: Berlin, 1986; pp 256.

0001-4842/92/0125-0227$03.00/0

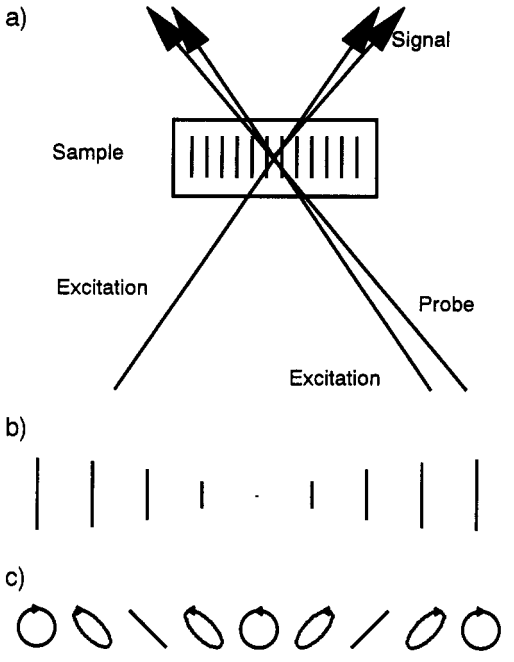

Figure 1. (a) TG experimental geometry. The excitation beams are crossed at an angle and temporally and spatially overlapped, creating a spatial inteference pattern that writes a grating (volume hologram) into the medium being studied. The probe beam is brought in at delay time t at the grating Bragg angle; the resultant diffracted signal is recorded as a function of t. (b) Electric-field picture for a single fringe of an IG (in which the excitation beams have parallel polarizations). The polarization of the electric field is constant across the grating, but the field amplitude is sinusoidally modulated. (c) Electric-field picture for a single fringe of a PG (in which the excitation beam have perpendicular polarizations). The electric field is of constant amplitude across each fringe, but changes in polarization from rcp to −45° linear to lcp to +45° linear and back to rcp across each fringe.

phases of matter and have been used to probe phenomena as diverse as rotational rates in liquids,[8] exciton transport in crystals,[9] electron transport in semiconductors,[10] phase transitions,[11] acoustic wave propagation in bulk materials,[12] and semiconductor–liquid interfaces.[13] Here we describe three recent applications of the TG to problems in chemical physics: the study of picosecond dynamics in flames (a gas-phase example), femtosecond to nanosecond dynamics of complex molecular liquids (a liquid-phase example), and the measurement of heat flow in and acoustic properties of thin films (a solid-phase example).

To form a TG, two time-coincident laser pulses of wavelength λ are crossed at an angle θ in a medium. The electric fields of these excitation beams interfere with one another, resulting in a spatially-modulated net electric field [with a fringe spacing of $d = \lambda/[2 \sin(\theta/2)]$ in the beam-crossing volume (Figure 1a). The interference pattern can then interact with the medium through mechanisms such as absorption, the optical Kerr effect (OKE), and stimulated Brillouin scattering. This interaction in turn produces a periodic spatial modulation in the complex index of refraction of the medium, thereby creating what is, in essence, a temporary volume hologram (diffraction grating). If, after some delay time t, a probe laser beam is brought in such that it meets the grating at the Bragg angle, part of the beam will be diffracted. The strength of the diffracted signal is directly related to the depth of the induced grating (i.e., the peak/null difference in the complex index of refraction) and is monitored as a function of t. The TG signal is sensitive to any time-dependent process that can affect the spatial modulation of the complex index of refraction.

The polarizations of the excitation beams determine the dynamic processes to which the TG decay is sensitive. These beams are most commonly of either parallel linear polarizations, forming what is called an intensity grating (IG), or perpendicular linear polarizations, forming what is called a polarization grating (PG). The IG electric field is of the same polarization throughout, but is modulated sinusoidally in amplitude across each grating fringe (Figure 1b). The IG signal beam is in general of the same polarization as the beam used to probe the grating. The PG electric field is constant in amplitude, but its polarization is spatially modulated; the polarization changes from right circularly polarized (rcp) to linearly polarized at −45° (m or minus) to left circularly polarized (lcp) to linearly polarized at +45° (p or plus) and then back to rcp across each fringe, with elliptical polarizations interspersed in between (Figure 1c). If the polarization of the beam used to probe a PG is parallel to the polarization of one of the excitation beams, then the signal beam is polarized parallel to the other excitation beam.

Because the IG electric field is a sinusoidal modulation, it is easy to understand both how the IG diffracts light and how it decays. Any process that causes the grating peaks to lose population and/or the grating nulls to gain population will wash out the grating and, therefore, cause the diffracted signal to decrease. It is more difficult to see from electric-field pictures such as Figure 1c how a PG produces a signal, much less what causes this signal to decay. We have shown that any grating can be decomposed into a sum of IGs that have different spatial phases and different electric field polarizations; this scheme is called the grating decomposition method (GDM).[14] For instance, the PG can be decomposed into a rcp IG, an m-polarized IG that is 90° spatially out of phase with the rcp grating, an lcp IG that is 180° spatially out of phase with the rcp grating, and a p-polarized IG that is 270° spatially out of phase with the rcp grating.

The GDM provides ready explanations for many PG phenomena, such as why the polarization of the probe beam is rotated. Consider a PG experiment performed in an isotropic, absorbing liquid. It is straightforward to show that the circularly-polarized component gratings do not contribute to the signal, so only the two linearly-polarized gratings need to be considered.[14] Any linear probe beam polarization can be broken up into p- and m-polarized components. The p-polarized com-

(7) Fayer, M. D. *Annu. Rev. Phys. Chem.* **1982**, *33*, 63–87.
(8) Hyde, P. D.; Evert, T. E.; Ediger, M. D. *J. Chem. Phys.* **1990**, *93*, 2274.
(9) Rose, T. S.; Righini, R.; Fayer, M. D. *Chem. Phys. Lett.* **1984**, *106*, 13–19.
(10) Kasinski, J. J.; Gomez-Jahn, L.; Min, L.; Bao, Q.; Miller, R. J. D. *J. Lumin.* **1988**, *40-41*, 555.
(11) Farrar, M. R.; Cheng, L.-T.; Ya, Y.-X.; Nelson, K. A. *IEEE J. Quantum Electron.* **1986**, *QE-22*, 1453.
(12) Fayer, M. D. *IEEE J. Quantum Electron.* **1986**, *QE-22*, 1437–1452.
(13) Kasinski, J. J.; Gomez-Jahn, L. A.; Faran, K. J.; Gracewski, S. M.; Miller, R. J. D. *J. Chem. Phys.* **1989**, *90*, 1253.
(14) Fourkas, J. T.; Trebino, R.; Fayer, M. D. *J. Chem. Phys.*, in press.

ponent sees the greatest change in optical density at the maxima of the p-polarized component grating (i.e., the minima of the m-polarized grating) and the least change at the minima of this grating (the maxima of the m-polarized grating). The situation is reversed for the m-polarized component. Because the p- and m-polarized component gratings are spatially 180° out of phase with one another, a 180° phase shift is induced between the corresponding components of the probe beam. Thus, for instance, an x-polarized ($p + m$) probe beam produces a y-polarized ($p - m$) signal beam.

In many chemical problems, the TG offers distinct advantages over more common techniques. Because the signal is diffracted in a unique direction, the TG is a zero-background technique (as compared to pump–probe spectroscopy, for example). Excellent signal-to-noise (S/N) ratios can be obtained over many orders of magnitude of signal strength; thus, the TG is better suited to probing picosecond or femtosecond phenomena than are its frequency-domain analogues, such as nearly-degenerate four-wave mixing (NDFWM)[15] and dynamic light scattering (DLS).[16] The TG is noninvasive, so that dynamic processes can be monitored without actual physical contact. Finally, the polarization-selective aspect of the TG makes it possible to isolate and measure different phenomena in a single system. We will illustrate these points in the following experimental examples.

Picosecond Dynamics of Sodium-Seeded Flames

Combustion is an extraordinarily complex process. Hundreds of chemical reactions take place in all but the simplest of flames.[17] To further complicate matters, the chemical species and reactions that are prevalent depend greatly on which region of the flame is being probed. Different regions communicate with one another through transport and collisions, processes that take place on nanosecond or picosecond time scales. Therefore it is desirable in the study of combustion to be able to probe picosecond dynamics noninvasively and as a function of location.

We have recently demonstrated that the TG is a useful tool for such studies. We have monitored the transport and population dynamics of sodium atoms in various premixed flames using picosecond, polarization-selective TG experiments.[18,19] The TG is most useful in measuring gas-phase transport when the mean free path of the species of interest is either much larger or much smaller than the grating fringe spacing.[20,21] We describe here experiments in the latter regime, in which the signal decay is proportional to $\exp[-2t(\Delta^2 D + 1/\tau)]$, where Δ is $2\pi/d$, D is the diffusion constant of the species, and τ is the excited-state lifetime.

Figure 2a shows an IG decay in a Na-seeded, methane/air flame at a fringe spacing of 13.6 μm. The decay is exponential, with a decay time of 400 ps (corresponding to a decay constant of 800 ps). The grating was excited from the ground (3S) level to the $3P_{1/2}$ level and probed from the ground level to the $3P_{3/2}$ level. The IG decays in this flame look essentially identical over a large range of fringe spacings (from 5 μm to 20 μm). This demonstrates that the lifetime term dominates the decay; i.e., all of the Na atoms return to the ground state before there is time for diffusion to affect the grating significantly. Since the natural Na excited-state lifetime is 16 ns,[22] the observed 800-ps lifetime is the result of collisional quenching. There are many species in methane/air flames that are known to be good Na excited-state quenchers, and 800 ps is in good agreement with previous quenching-time measurements.[23-25]

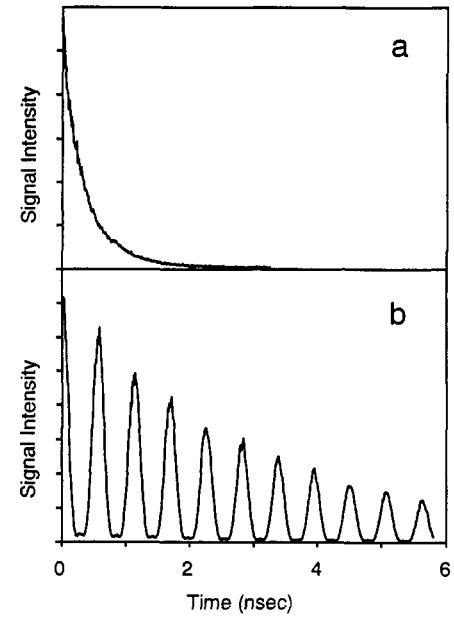

Figure 2. (a) IG decay in a methane/air flame at a fringe spacing of 13.6 μm. The D_1 line was excited and the D_2 line probed. The decay is exponential, with a decay time of 400 ps. (b) PG decay under the same conditions. The decay shows large beats at the 1.77-GHz Na ground-state hyperfine-splitting frequency, as well as small beats at twice this frequency. The decay has an exponential envelope with a 2.8-ns decay time. (After ref 18.)

Figure 2b shows PG data taken under the same conditions. The differences between the IG and PG decays are striking. The PG decays exhibit large oscillations at the 1.77-GHz ground-state hyperfine-splitting frequency (and smaller oscillations at twice this frequency). Although the envelope of the PG decay is exponential, the decay time is much longer than that of the IG. At the 13.6-μm fringe spacing shown here, the PG decay time is 2.8 ns, 7 times longer than that of the IG decay. Furthermore, a plot of the PG decay constant versus Δ^2 gives a straight line with a nonzero slope, as would be expected if diffusion were dominating the decay. The slope of this line yields a diffusion constant of 4.3 ± 0.5 cm^2/s. The y-intercept of this plot indicates that there is an additional grating decay process with a 6-ns lifetime.

With the aid of the GDM, we have been able to understand and interpret these data by considering what

(15) Trebino, R.; Barker, C. E.; Siegman, A. E. *IEEE J. Quantum Electron.* **1986**, *QE-22*, 1413–1430.
(16) Berne, B. J.; Pecora, R. *Dynamic Light Scattering*; Wiley: New York, 1976.
(17) Glassman, J. *Combustion*; Academic Press: Orlando, 1987.
(18) Fourkas, J. T.; Brewer, T. R.; Kim, H.; Fayer, M. D. *Opt. Lett.* **1991**, *16*, 177–179.
(19) Fourkas, J. T.; Brewer, T. R.; Kim, H.; Fayer, M. D. *J. Chem. Phys.* **1991**, *95*, 5775–5784.
(20) Rose, T. S.; Wilson, W. L.; Wäckerle, G.; Fayer, M. D. *J. Phys. Chem.* **1987**, *91*, 1704–1707.
(21) Rose, T. S.; Wilson, W. L.; Wäckerle, G.; Fayer, M. D. *J. Chem. Phys.* **1987**, *86*, 5370–5391.
(22) Kibble, B. P.; Copley, G.; Krause, L. *Phys. Rev.* **1967**, *153*, 9–12.
(23) Russo, R. E.; Hieftje, G. M. *Appl. Spectrosc.* **1982**, *36*, 92.
(24) Takubo, Y.; Okamoto, T.; Yamamoto, M. *Jpn. J. Appl. Phys.* **1985**, *24*, L263–L265.
(25) Alfano, A. J. *Appl. Opt.* **1989**, *25*, 5010.

happens to the ground-state magnetic sublevel populations when the grating is created and as population is quenched from the excited state.[14,19] We have developed a detailed theoretical model that both explains the insensitivity of the PG decay to excited-state quenching and predicts the proper functional form for the decay. In addition, this model shows that the process corresponding to the 6-ns decay time in the PG is the scattering of population among the ground-state sublevels. This scattering rate has never before been measured in flames.

The results of these preliminary experiments are encouraging. With modern laser technology, tunable pulses with picosecond or femtosecond time resolution can be obtained, so it should be possible to use the TG technique to study the fast dynamics of virtually any combustion species. The TG promises to be of great value in combustion research, as well as in the study of plasmas and other gas-phase systems.

Dynamics of Simple and Complex Molecular Liquids

The dynamics of molecules in simple and complex liquids are of fundamental interest to chemists. Various spectroscopic methods have been developed to monitor either single-molecule or bulk correlation functions in liquids. With the advent of high-power, picosecond and femtosecond laser systems, it is possible to measure these correlation functions directly. This can be accomplished by performing TG optical Kerr effect (TG-OKE) experiments.[26]

The OKE contains both an electronic and a nuclear component. The former is the instantaneous distortion of the electron cloud of a molecule due to an incident light electric field; this effect disappears when the light is removed, so there is no electronic OKE (e-OKE) signal once the excitation pulses are over. The nuclear OKE (n-OKE) is the rotation of molecules as they attempt to minimize the energy of the interaction between their polarizability and the incident electric field. The excitation pulses thus create a small net alignment of the molecules, which in turn forms a polarization-dependent grating in the real part of the index of refraction. The probe pulse monitors the decay of this induced birefringence as the molecules return to an equilibrium, isotropic state. Thus, the TG-OKE technique is a sensitive probe of ultrafast orientational relaxation.[27,28] Note that the TG-OKE is a nonresonant experiment. Because only the real part of the index of refraction is probed, an OKE grating can be created and probed at any wavelength; compare this to the Na experiments described above, in which the gratings were created solely in the imaginary part of the index of refraction.

Both DLS and TG-OKE experiments probe bulk orientational correlation functions. Yan and Nelson have shown that a DLS experiment with infinite frequency resolution is the Fourier transform of a TG-OKE experiment with infinite time resolution.[29,30] However, in practice it is difficult to monitor ultrafast

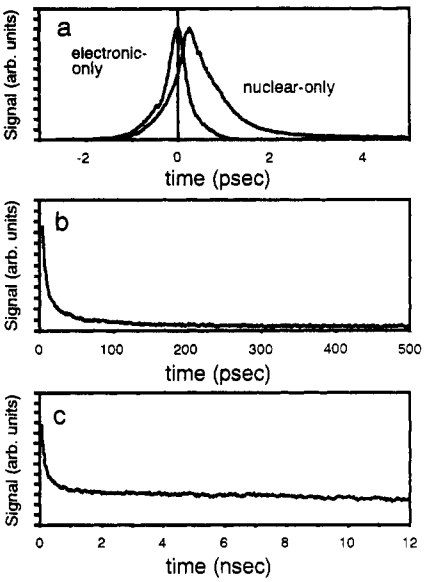

Figure 3. TG-OKE data in neat 5CB at 41.7 °C on (a) fast, (b) intermediate, and (c) slow time scales. Two sets of data are shown in part a, one in which the e-OKE response has been suppressed and one in which the n-OKE response has been suppressed. (After ref 32.)

dynamics using DLS, whereas the TG-OKE technique can monitor dynamics on time scales from femtoseconds to tens of nanoseconds with excellent S/N ratios. Here we will discuss TG-OKE investigations of 4-*n*-pentyl-4′-cyanobiphenyl (5CB),[27,31,32] which can exist in different liquid crystalline phases.

If one is to be able to obtain unambiguous information on orientational relaxation, the n-OKE should ideally be the only effect contributing to the grating signal. However, even if the excitation and probe wavelengths are carefully chosen such as to avoid any kind of absorptive effects, the e-OKE response will still obscure the n-OKE response at short delays. This problem can be overcome by taking advantage of the symmetry properties of the e- and n-OKE to select a set of beam polarizations such that one or the other effect disappears;[27,33] this is illustrated for 5CB in Figure 3a. These polarization angles can be derived either directly from the nonlinear refractive index or by using the GDM.

How local structure influences dynamics is a fundamental question in the study of liquids. To address this question, the isotropic liquid crystalline phase of 5CB was investigated. The strong tendency of 5CB molecules to align with one another results in a high degree of local order, even in the isotropic phase. Within 10 or 20 °C of the phase transition, locally-ordered regions exist. These domains increase in size as the temperature is reduced. As a result, 5CB exhibits dynamics that are vastly different from those of biphenyl, its parent molecule. This is illustrated in Figure 3, which shows the dynamics of neat 5CB at 41.7 °C (which is above the nematic/isotropic phase transition).[32] Figure 3a shows the early-time (<5 ps) dynamics; following the fast librational dynamics, the data appear almost flat

(26) Eyring, G.; Fayer, M. D. *J. Chem. Phys.* **1984**, *81*, 4314–4321.
(27) Deeg, F. W.; Fayer, M. D. *J. Chem. Phys.* **1989**, *91*, 2269–2279.
(28) Ruhman, S.; Williams, L. R.; Joly, A. G.; Nelson, K. A. *Chem. Phys. Lett.* **1987**, *141*, 16–24.
(29) Yan, Y. X.; Cheng, L. F.; Nelson, K. A. *Adv. Infrared Raman Spectrosc.* **1987**, *16*, 299.
(30) Yan, Y. X.; Nelson, K. A. *J. Chem. Phys.* **1987**, *87*, 6240.
(31) Deeg, F. W.; Stankus, J. J.; Greenfield, S. R.; Newell, V. J.; Fayer, M. D. *J. Chem. Phys.* **1989**, *90*, 6893–6902.
(32) Deeg, F. W.; Greenfield, S. R.; Stankus, J. J.; Newell, V. J.; Fayer, M. D. *J. Chem. Phys.* **1990**, *93*, 3503–3514.
(33) Etchepare, J.; Grillon, G.; Chambaret, J. P.; Hamoniaux, G.; Orszag, A. *Opt. Commun.* **1987**, *63*, 329–334.

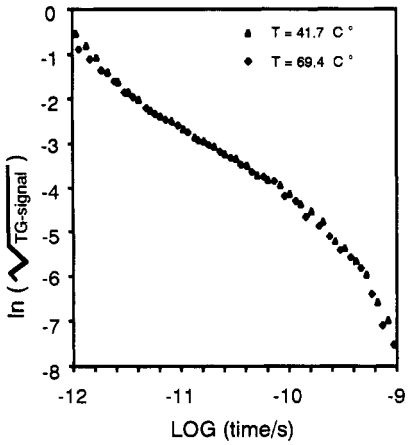

Figure 4. Fast- and intermediate-time-scale dynamics of neat 5CB at 41.7 and 69.4 °C. The slow processes have been fit and subtracted from the data. Note that the plots fall on top of one another, even though the viscosity changes by a factor of 3 over this temperature range. (After ref 32.)

on this time scale. Figure 3b illustrates the intermediate-time-scale dynamics (out to 500 ps); the fast decay component in this plot is the slow decay component from the previous plot. Figure 3c shows the long-time-scale dynamics (out to 12 ns); the fast decay at short times in Figure 3c is the nearly flat component in Figure 3b. Only the slowest data (>1 ns) are exponential. The data in between the librational decay and the slow decay (from 1 pst to 1 ns) cannot be fit to any simple sum of exponentials.

The behavior of the slow (>1 ns) decay component with temperature is consistent with Landau–deGennes theory over a temperature range of about 35 °C. According to this theory, the slow decay corresponds to the randomization of local pseudonematic domain structure. At about 70 °C, the dynamics begin to deviate from Landau–deGennes behavior. At this temperature, the domain correlation length is only 2–3 molecular lengths, and the pseudonematic domains cease to exert influence on the liquid dynamics.

The fast-time-scale (1 ps to 1 ns) dynamics in this system are extremely interesting. Plotted in Figure 4 is the natural logarithm of the square root of the fast-time-scale data; the slow exponential terms (pseudonematic-domain decay) have been subtracted from the square root of the data. [When the slow decay components are included, these data cover both 5 orders of magnitude of time scales (from hundreds of femtoseconds to tens of nanoseconds) and more than 20 factors of e (8 orders of magnitude) in signal intensity, yet the S/N ratio is excellent throughout.] This is actually a plot of data taken at two different temperatures, 41.7 and 69.4 °C; although the bulk viscosity is reduced by a factor of 3 in going from 41.7 to 69.4 °C, these data sets fall right on top of one another. The fast dynamics are independent of temperature (and viscosity) over a range in which the time constant for the slow, collective dynamics changes by an order of magnitude. This lack of temperature dependence is in sharp contrast to the behavior of simple liquids such as biphenyl.

The fact that the fast dynamics are independent of temperature over such a large range is very important. Such behavior is clearly nonhydrodynamic.[32] Consider a single local structure that, on the time scale of the fast dynamics, is essentially fixed. Before the laser pulses, the structure resides in a local minimum of the collective free energy potential surface. The excitation electric field moves the system away from this minimum by slightly altering the relative molecular orientations. The system then relaxes along the potential surface and returns to a local minimum. The system cannot undergo diffusive randomization on a time scale that is fast compared to the time scale for the loss of local structure, and therefore changes in the viscosity of the system with temperature are unimportant. The dynamics are controlled by details of the intermolecular interactions of the local structure. Analogous behavior has recently been observed in a conventional liquid.[34]

Heat Flow and Acoustic Properties of Thin-Film, High-Temperature Superconductors

Having discussed applications of the TG in gas- and liquid-phase systems, we now turn to solid-phase TG experiments. In particular, we will discuss the use of the TG techniques to investigate the heat flow and acoustic properties of thin films of $YBa_2Cu_3O_{7-x}$ (YBCO), a high-temperature superconductor, without necessitating physical contact with the material.[35] These experiments illustrate the ability of the TG technique to probe selectively either surface or bulk phenomena.[36]

The experiments described here were performed on thin-film samples of YBCO grown on an optically transparent substrate of MgO. The grating excitation in these experiments was made at a wavelength at which YBCO is highly absorbing. Electronic excitations in YBCO are transformed into heat in approximately 1 ps; this heat causes thermal expansion in the medium, with the greatest expansion occurring at the peaks of the grating. The spatially-modulated thermal expansion changes the index of refraction of the medium, giving rise to a thermal grating. The grating signal is washed out as the heat diffuses from the grating peaks to the grating nulls. The thermal expansion also launches acoustic waves in the sample, thereby producing oscillations in the signal.[12] Because the YBCO sample is thin, it acts as a waveguide. The fringe spacing determines which waveguide modes are excited; several modes may be excited at a given fringe spacing.[37] The damping times for each of these acoustic modes can be determined from the manner in which the oscillations in the signal decay.

Illustrated in Figure 5 are TG data taken on a 220-nm-thick YBCO sample at a temperature of 296 K. The data were taken in four different geometries, each of which is labeled next to the corresponding decay. The letters "T" and "R" stand for transmission and reflection geometries, respectively. In the transmission geometry, the signal beam travels through the sample before it is detected, and in the reflection geometry, the signal beam is detected on the side of the sample upon which the three laser beams are incident. The letters "a" and "b" specify the side of the sample on which the

(34) Greenfield, S. R.; Stankus, J. J.; Sengupta, A.; Fayer, M. D. *Chem. Phys. Lett.*, in press.
(35) Marshall, C. D.; Fishman, I. M.; Fayer, M. D. *Phys. Rev. B*, in press.
(36) Fishman, I. M.; Marshall, C. D.; Meth, J. S.; Fayer, M. D. *J. Opt. Soc. Am. B: Opt. Phys.* **1991**, *8*, 1880–1888.
(37) Meth, J. S.; Marshall, C. D.; Fayer, M. D. *J. Appl. Phys.* **1990**, *67*, 3362–3377.

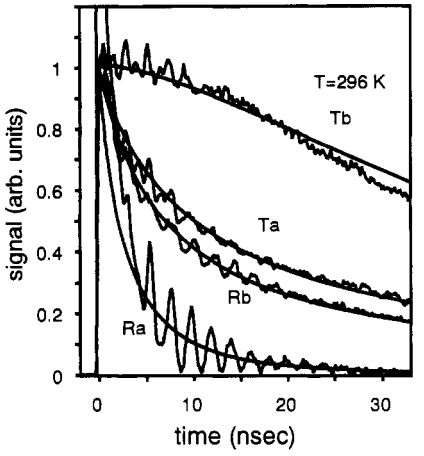

Figure 5. TG decays at 300 K in 220-nm-thick YBCO film on a MgO substrate. The smooth lines are fits to the data, excluding acoustic waves. T = transmission geometry, R = reflection geometry, a = beams incident on the YBCO/MgO interface side of the film, b = beams incident on the YBCO/vacuum side of the film. (After ref 35.)

grating is created; the YBCO/MgO interface is denoted by "a", whereas the YBCO/vacuum interface is denoted by "b".

It can be seen from Figure 5 that both the heat flow and acoustic portions of the decays vary significantly depending on the experimental geometry used. Recent theoretical work[36] has demonstrated that TG experiments can be surface or interface selective. The transmitted signal probes the bulk of a sample. However, in a sample that is either nonabsorbing or has a Beer's length much longer than the optical wavelength of the experimental beams, the reflected signal is sensitive strictly to the interface or surface dynamics. If the Beer's length is on the order of the wavelength of the light, the grating will probe the material to a somewhat greater depth (on the order of one-half the Beer's length).

The differences in the signal decays when different faces are probed arise from contact between the sample and the MgO substrate. At small fringe spacings, the TG signal is much more sensitive to diffusion parallel to the film than to diffusion perpendicular to the film. At large fringe spacings, the signal is sensitive only to perpendicular diffusion and flow into the substrate. Thus, both heat flow into the substrate and the anisotropy in thermal diffusion can be measured. If the grating is created at the interface, the perpendicular diffusion can occur in two directions: into the YBCO film and into the substrate. Under the experimental conditions, heat in the substrate does not contribute to the signal. On the other hand, if the grating is created at the vacuum face of the YBCO, perpendicular diffusion can only occur into the film, and the signal will only decay once diffusion has carried the heat across the film and into the substrate.

By using the four types of curves displayed in Figure 6, it is possible to characterize completely the heat flow into a thin film, as well as the flow from the film into the substrate. The smooth lines in Figure 5 are fits to the heat flow portion of the signals. Analysis of the data demonstrates that there is a substantial barrier to heat flow between the film and the substrate;[35] at room temperature, heat flow across the interface is 100 times slower than the diffusion in the film itself. This can

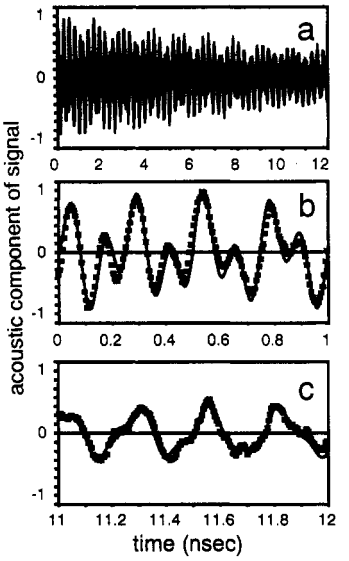

Figure 6. (a) Acoustic portion of TG decay in 350-nm-thick YBCO film at 300 K. The data is fit to two damped acoustic modes, one at 3.3 GHz and one at 8.3 GHz. (b) Blowup of signal (squares) and fit (solid line) starting at 0-ns delay time. (c) Blowup of signal and fit starting at 11-ns delay time. The same fitting parameters are used throughout. (After ref 35.)

be explained in terms of the molecular structure of the interface. The YBCO makes poor mechanical contact with the MgO.[38] This in turn results in poor thermal contact at the interface, which shows up as a large barrier to heat flow between the two materials. This type of barrier phenomenon has important implications for thin film device applications.

The TG data also yield the thermal diffusion constants parallel (D_{ab}) and perpendicular (D_c) to the plane of the film. Measurements of these constants and of the magnitude of the thermal barrier were made at temperatures ranging from 17 to 300 K. At room temperature, D_{ab} is 0.023 cm^2/s and D_c is 0.0028 cm^2/s.

Conventional methods of measuring acoustic properties work poorly on thin films, in part because of the need to have a transducer in physical contact with the sample. In many instances the TG is ideal for studying such properties. Figure 6a shows the acoustic portion of a TG decay in a 350-nm-thick sample at 300 K; the fringe spacing is 0.75 μm. The data are fit to two acoustic modes, one at 3.3 GHz and one at 8.3 GHz. The fit is so good that it cannot be seen in Figure 6a. The quality of the fit is illustrated by parts b and c of Figure 6, which are 1-ns blowups of both the data and the fit, starting at delay time of 10 and 11 ns, respectively. Analysis of the type of data provides elastic constants and acoustic damping parameters.

Conclusions

The TG is a powerful technique for studying fast dynamic processes, as it offers the combined advantages of background-free detection, large dynamic range, polarization selectivity, and the ability to probe phenomena over variable distance scales. We have discussed three applications of the TG technique, one in each phase of matter. Given a small bag of polarization, wavelength, and geometry tricks, it is possible to probe in detail a wide variety of fast phenomena. Although

(38) Streiffer, S. K.; Lairson, B. M.; Eom, C. B.; Clemens, B. M.; Bravman, J. C.; Geballe, T. H. *Phys. Rev. B* **1991**, *43*, 13007–13018.

once esoteric, the TG technique is now coming into its own, and it will find a wide variety of chemical applications in the coming years.

We thank the various persons who contributed to the work detailed in this Account. The GDM was developed in conjunction with Dr. Rick Trebino. The flame data were taken with the assistance of Timothy R. Brewer and Dr. Hackjin Kim, and the experiments were sponsored by the Office of Naval Research, Physics Division (N00014-89-J-1119). The TG-OKE experiments were performed by Dr. Fred Deeg, Dr. Vince Newell, Scott Greenfield, and John Stankus and were sponsored by the National Science Foundation, Division of Materials Research (DMR-9022675), and the Office of Naval Research, Physics Division (N00014-89-J-1119). The YBCO experiments and theory were developed by Chris Marshall and Dr. Ilya Fishman, and were sponsored by the NSF, Division of Materials Research (DMR-9022675); additional support was provided by the ONR (N00014-89-J-1119 and N00014-91-C-0170). J.T.F. thanks the NSF for a graduate fellowship.

Mechanistic and Synthetic Aspects of Amine–Enone Single Electron Transfer Photochemistry

UNG CHAN YOON

Department of Chemistry, College of Natural Sciences, Pusan National University, Pusan 609-735, Korea

PATRICK S. MARIANO*

Department of Chemistry and Biochemistry, University of Maryland—College Park, College Park, Maryland 20742

Received November 25, 1991

The recognition that single electron transfer (SET) can be a dominant reaction pathway followed when electronic excited state species interact with ground-state donors or acceptors has had a profound impact on the field of organic photochemistry. This has been especially important in the design, mechanistic analysis, and synthetic applications of new photochemical reactions. Both theoretical[1] and empirical relationships[2] now available enable an accurate estimation of the rate constants (k_{SET}) for excited-state SET based on experimentally measured redox potentials and excited-state energies. Consequently, relative efficiencies of SET versus other excited state decay pathways can be evaluated. In addition, SET between neutral excited donor–acceptor pairs leads to generation of ion radicals, intermediates which can undergo rapid, novel, and frequently predictable reactions to produce secondary radical or charged intermediates in routes for product formation.[3] In contrast to classical photochemical reactions where the pathways followed are governed by the characteristic bonding properties in excited states, the nature of excited-state SET reactions is controlled primarily by the chemistry of the ion radical intermediates. As a result, it is not surprising that the majority of new organic photochemical processes discovered in recent years operate via SET mechanisms and that a large number of these have found their way into the organic synthetic repertoire.[4]

Scheme I

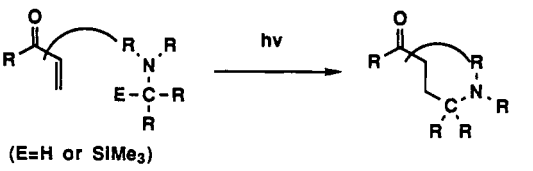

Scheme II

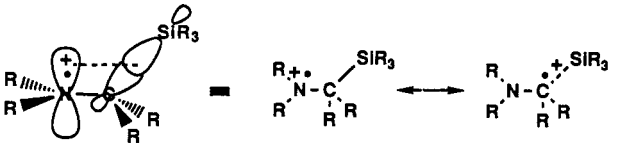

This Account focuses on a class of SET photochemical processes that we have explored extensively. The specific reactions involve photoadditions and photocyclizations of α,β-unsaturated ketone–tertiary amine systems (Scheme I). In reviewing the key observations, we will attempt to demonstrate how an understanding of the factors governing SET reaction efficiencies and ion radical chemistry can be used to mechanistically analyze new excited-state SET processes and to develop their synthetic potential. To establish the background

Ung Chan Yoon was born in Seoul and raised in Pusan, Korea. He received his B.S. and M.S. degrees in pharmacy at Seoul National University under the direction of Professor Young Eun Kim. After working with Professor Byung Hoon Han for one year at the Natural Products Research Institute of Seoul National University, Professor Yoon came to the United States to conduct his doctoral studies at Fordham University with Gary A. Epling. After postdoctoral work with Patrick S. Mariano at Maryland, he joined the faculty at Pusan National University, where he is now associate professor of chemistry. His research investigations are in the area of organic photochemistry.

Patrick S. Mariano was born and raised in New Jersey. He received his B.S. in chemistry at Fairleigh Dickinson University and his Ph.D. at the University of Wisconsin under the direction of Howard E. Zimmerman. After postdoctoral studies with Harry H. Wasserman at Yale, he joined the faculty at Texas A&M University in 1970, where he rose through the ranks and then in 1979 gained escape velocity when he accepted his current position as professor of chemistry and biochemistry at the University of Maryland, College Park. His investigations during the past decade have focused on organic photochemistry, synthesis, and bioorganic chemistry.

(1) Marcus, R. A. *J. Phys. Chem.* **1968**, *72*, 891. Scandola, F.; Balzani, V.; Schuster, G. B. *J. Am. Chem. Soc.* **1981**, *103*, 2519.
(2) Rehm, D.; Weller, A. *Isr. J. Chem.* **1970**, *8*, 259.
(3) Davidson, R. S. *Molecular Association*; Foster, R., Ed.; Academic Press: London, 1975; Vol. 1. Lablache-Combier, A. *Bull. Soc. Chim. Fr.* **1972**, *12*, 4791. Davidson, R. S. *Adv. Phys. Org. Chem.* **1983**, *19*, 1. Julliard, M.; Chanon, M. *Chem. Rev.* **1983**, *83*, 425.
(4) Mariano, P. S.; Stavinoha, J. L. *Synthetic Organic Photochemistry*; Horspool, W. M., Ed.; Plenum Press: London, 1984.

0001-4842/92/0125-0233$03.00/0